Available online at www.sciencedirect.com
SCIENCE DIRECT
Journal of Catalysis 234 (2005) 401–413
JOURNAL OF CATALYSIS
www.elsevier.com/locate/jcat

Selective catalytic reduction of NO_2 with urea in nanocrystalline NaY zeolite

Gonghu Li, Conrad A. Jones, Vicki H. Grassian *, Sarah C. Larsen *

Department of Chemistry, The University of Iowa, Iowa City, IA 52242, USA

Received 24 March 2005; revised 23 May 2005; accepted 2 June 2005

Available online 10 August 2005

Abstract

In this study, the selective catalytic reduction (SCR) of NO_2 with urea in nanocrystalline NaY zeolite was investigated with in situ transmission Fourier transform infrared (FTIR) spectroscopy and solid-state nuclear magnetic resonance spectroscopy. At $T = 473$ K, the reaction rate for urea-SCR of NO_2 in nanocrystalline NaY zeolite was significantly greater than that in commercial NaY zeolite with a larger crystal size. In addition, a dramatic decrease in the concentration of undesirable surface species, including biuret and cyanuric acid, was observed in nanocrystalline NaY compared with commercial NaY after urea-SCR of NO_2 at $T = 473$ K. The increased reactivity for urea-SCR of NO_2 was attributed to silanol groups and extra-framework aluminum species located on the external surface of nanocrystalline NaY. Specifically, NO_x storage as nitrate and nitrite on the internal zeolite surface was coupled to reactive deNO_x sites on the external surface. Isotopic labeling combined with IR analysis suggest that N–N bond formation involved both an N-atom originating from NO_2 and an N-atom originating from urea. This is the first clear example demonstrating that the increased external surface area (up to ∼40% of total surface area) of nanocrystalline zeolites can be used as a reactive surface with unique active sites for catalysis.

Keywords: Selective catalytic reduction; NO_2; Y Zeolite; Urea; Isotopic labeling; Nanocrystals

1. Introduction

Selective catalytic reduction (SCR) using ammonia or hydrocarbons is a promising technology for post-combustion treatment of NO_x (NO and NO_2) [1]. NH_3-SCR has been developed and used worldwide for the control of NO_x emissions in fuel combustion from stationary sources due to its efficiency, selectivity, and economics [2]. However, NH_3 is not a practical reducing agent for NO_x emissions from mobile sources, because of its toxicity and difficulties in storage, transportation, and handling [1]. Much interest has focused on using urea as a safer source of ammonia in automotive applications [3–7]. Currently, a solution of 32.5% urea in water is the preferred choice among different precursors for ammonia [8–11]. It is generally accepted that urea thermally decomposes in two steps (reactions (1) and (2)) to form ammonia and carbon dioxide [12–14]:

$$(NH_2)_2CO \rightarrow NH_3 + HNCO, \quad (1)$$

$$HNCO + H_2O \rightarrow NH_3 + CO_2. \quad (2)$$

Transition metal-containing zeolites have been extensively studied as SCR catalysts [15–20]. Several recent studies have also used alkali and/or alkaline earth-substituted Y zeolites as selective oxidation catalysts [21–23] and deNO_x catalysts [24–29]. In the absence of transition metals, zeolite Y potentially offers novel SCR pathways different from those in transition metal containing catalysts. As recently discussed, nanocrystalline Y zeolites and metal oxides with particle sizes less than 100 nm may be particularly useful in environmental applications because of their small crystal sizes and large internal and external surface areas [30–33]. The influence of intracrystalline diffusion on SCR reaction rate has been previously investigated for transition metal-exchanged zeolites with different crystal sizes [34–38]. Most

* Corresponding authors. Fax: +1-319-335-1270.
E-mail addresses: vicki-grassian@uiowa.edu (V.H. Grassian), sarah-larsen@uiowa.edu (S.C. Larsen).

0021-9517/$ – see front matter
doi:10.1016/j.jcat.2005.06.025

applicable to the current study is recent work on propylene-SCR of NO_2 over nanocrystalline NaY zeolite with a crystal size of 23 nm [32]. At $T = 473$ K, significantly higher NO_x conversion and higher selectivity toward N–N bond formation was observed in nanocrystalline NaY zeolite compared with commercial NaY zeolite with a larger crystal size [32]. It was also observed that nanocrystalline NaY zeolite was more sensitive to the presence of adsorbed water than commercial NaY zeolite in propylene-SCR of NO_2 at $T = 473$ K [32]. The silanol groups and extra-framework aluminum (EFAL) species with Bronsted acidity located on the external surface of nanocrystalline NaY zeolite were found to account for the observed differences in activity (see Fig. S1 in Supplementary information [32]).

In the study reported here, in situ transmission FTIR spectroscopy was used to investigate urea-SCR of NO_2 over nanocrystalline NaY zeolite at relatively low temperature ($T = 473$ K). This work is motivated by the fact that the silanol groups and EFAL sites on the external surface of nanocrystalline NaY may be effective surface sites for the decomposition of urea to NH_3 and the subsequent SCR of NO_2 [2,8]. The performance of nanocrystalline NaY zeolite in urea-SCR reactions is compared to commercial NaY zeolite with a larger crystal size to explore the potential advantages of the small crystal size of nanocrystalline NaY zeolite and to determine whether the chemical and physical properties of nanocrystalline NaY are important in facilitating urea-SCR reactions.

2. Experimental section

2.1. Zeolite sample preparation and materials

Nanocrystalline NaY zeolite was synthesized using clear solutions according to the general method reported by Creaser et al. [39] and further modified by Song et al. [30]. Sodium hydroxide, aluminum isopropoxide, tetramethylammonium hydroxide (TMAOH), and distilled water were mixed and stirred until the resulting mixture became a clear solution. Then tetraethylorthosilicate (TEOS) was added to the clear solution. The clear solution mixture was stirred overnight to ensure complete hydrolysis of the aluminum and silicon sources. The final clear synthesis gel had the following composition: 0.07 Na:2.4 TMAOH:1.0 Al:2.0 Si:132 H_2O:3.0 i-PrOH:8.0 EtOH. The latter two alcohols were formed from the hydrolysis of aluminum isopropoxide and TEOS, respectively. To optimize the formation of small NaY crystals, the sodium content was intentionally set too low relative to the aluminum content in the synthesis gel. The clear solution was transferred into a 500-mL flask equipped with an air-cooled condenser and was heated to $T = 368$ K in an oil bath for 84 h with stirring. Nanocrystalline Y powders were recovered from the milky, colloidal suspension of NaY after two cycles of centrifugation, washed with deionized water, and dried at $T = 393$ K in air. The nanocrystalline NaY sample was calcined at $T = 773$ K under oxygen flow for 16 h to remove organic templates.

The synthesized nanocrystalline NaY zeolite and the commercial NaY zeolite (purchased from Aldrich) were characterized by several different techniques, including scanning electron microscopy (SEM), X-ray diffraction, nitrogen adsorption isotherms, and solid-state nuclear magnetic resonance (NMR) [30]. The average crystal size of nanocrystalline NaY zeolite was determined to be 23 nm [30]. The commercial NaY zeolite is composed of large intergrown NaY crystals with diameters of ∼1 μm. The external, internal, and total surface areas of nanocrystalline NaY zeolite were determined to be 178, 406, and 584 m^2/g, respectively. The total surface area of commercial NaY zeolite was 477 m^2/g, and, as discussed in previous work [30], the external surface area of commercial NaY zeolite is estimated from the crystal size to be ∼4 m^2/g. The Si/Al ratios of nanocrystalline NaY and commercial NaY zeolite were determined to be 1.8 and 2.0, respectively [30].

Aluminum isopropoxide, TEOS, and sodium hydroxide were purchased from Alfa Aesar. Commercial NaY zeolite and TMAOH solution (20 wt%) were purchased from Aldrich. Solid urea (>99.5%) was purchased from Acros Organics. ^{15}N- and ^{13}C-labeled urea were purchased from Cambridge Isotopes. Research-grade purity oxygen and carbon dioxide were purchased from Air Products. Anhydrous ammonia, research-grade purity nitrogen dioxide, nitric oxide, and nitrous oxide were purchased from Matheson. All gases were used without further purification.

2.2. Transmission FTIR spectroscopy

Four mg urea in aqueous solution (∼0.3 mol) and 7 mg NaY zeolite were mixed and sonicated for 30 min at room temperature. The resulting hydrosol was coated onto a 3 × 2 cm tungsten grid held in place by nickel jaws. The nickel jaws were attached to copper leads so that the sample could be resistively heated. A thermocouple wire attached to the tungsten grid was used to measure the temperature of the sample. The tungsten grid with zeolite sample was placed inside a stainless steel cube, which had two BaF_2 windows for FTIR measurements and was connected to a vacuum/gas handling system [23].

The stainless steel FTIR cell was held in place by a linear translator inside the sample compartment of a Mattson Galaxy 6000 FTIR spectrometer equipped with a narrow-band MCT detector. The linear translator allowed each half of the sample grid to be moved into the FTIR beam path, permitting detection of gas phase and adsorbed species in zeolites under identical reaction conditions. Each absorbance spectrum shown was obtained by referencing 64 scans at an instrument resolution of 4 cm^{-1} to the appropriate background of the zeolite or the blank grid, unless noted otherwise.

The NaY zeolite sample with adsorbed urea was dried in air and evacuated at room temperature overnight to remove

weakly adsorbed water. Reactant gases (NO_2 and O_2) were loaded into the NaY zeolite through the gas handling system. Two absolute pressure transducers were used to monitor the pressure. The extinction coefficients of individual gases were calibrated using the characteristic FTIR absorption band and measuring the pressure using an absolute pressure transducer. Typically, the NaY zeolite was equilibrated with gases before a spectrum was recorded. In SCR reactions, NO_2 was first introduced into the FTIR cell at room temperature. After 30 min to allow adsorption equilibrium, an excess amount of oxygen was added into the FTIR cell. Time course experiments were conducted by automatically recording FTIR spectra of the gas phase every 1 min.

2.3. Solid-state magic-angle spinning NMR experiments

Approximately 200 mg of zeolite were impregnated with an aqueous solution of labeled urea (^{13}C and ^{15}N). Samples with adsorbed urea were allowed to dry at room temperature and were placed into Pyrex sample tubes that were degassed on a vacuum rack. To prepare samples containing labeled urea and nitric oxide and oxygen, the nitric oxide and oxygen were introduced to the zeolite sample while still attached to the vacuum rack. Then the Pyrex sample tube was sealed while the sample was immersed in liquid nitrogen. The sealed samples were heated for 1 h at the desired temperatures. Samples were allowed to cool to room temperature for the NMR measurements.

Magic-angle spinning (MAS) NMR spectra were obtained using a 7-Tesla wide bore Bruker cryomagnet and a TecMag Discovery console. The Larmour frequencies for ^{13}C and ^{15}N were 75.470 and 30.425 MHz, respectively. A Chemagnetics double-channel 7.5-mm pencil MAS probe was used to spin rotors containing the sealed samples. The spinning speed was approximately 4.0 kHz. Single-pulse direct excitation was used for ^{13}C and ^{15}N. The $\pi/2$ pulse width was 6.0 μs for ^{13}C; the $\pi/2$ pulse width was 4.5 μs for ^{15}N. Recycle delay was 2 s, and a line broadening of 50 Hz was used for both ^{13}C and ^{15}N. There were 4000 scans for the ^{13}C NMR and 25,000 scans for the ^{15}N MAS NMR. Solid adamantane mixed with KBr (38.5 ppm) and saturated $^{15}NH_4{}^{15}NO_3$ solution (0 ppm for $NO_3{}^-$) were used as external chemical shift standards for ^{13}C and ^{15}N, respectively. All of the chemical shifts for ^{13}C and ^{15}N are reported relative to TMS and CH_3NO_2, respectively. All ^{13}C and ^{15}N spectra were obtained at room temperature.

3. Results

3.1. Adsorption of NO_2 in NaY zeolite with adsorbed urea at $T = 298$ K

As discussed earlier, an aqueous urea solution and the NaY zeolite powder were mixed at room temperature. Before adsorbing NO_2, the NaY zeolite sample with area was dried in air and evacuated at room temperature overnight to remove weakly adsorbed water. The FTIR spectrum of commercial NaY zeolite with adsorbed urea is shown in Fig. 1. The FTIR spectrum of a clean commercial NaY sample is also plotted in Fig. 1 (dotted line) for comparison.

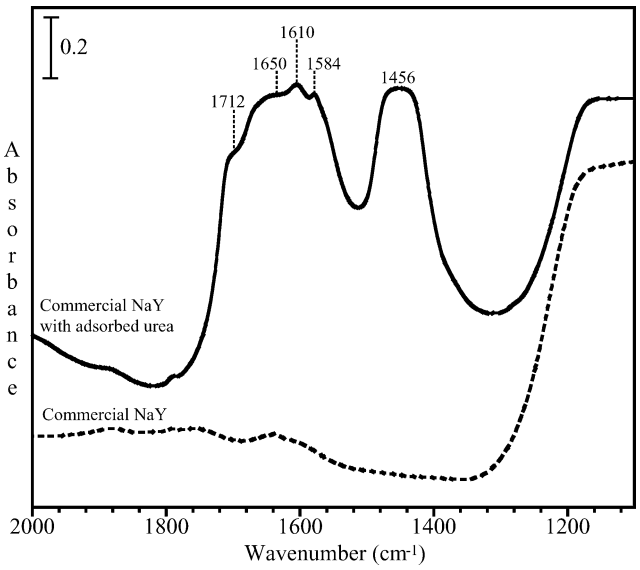

Fig. 1. FTIR spectrum of commercial NaY with adsorbed urea at $T = 298$ K. The zeolite sample with adsorbed urea was dried in air and evacuated at $T = 298$ K overnight. The FT-IR spectrum of a clean commercial NaY sample is also plotted (dotted line). The blank grid is used as a reference. All spectra were recorded at $T = 298$ K.

Adsorbed urea in NaY zeolite can be identified by several absorption bands at 1456, 1584, 1610, 1650, and 1712 cm^{-1} in the FTIR spectrum as shown in Fig. 1. The absorption band at 1456 cm^{-1} is assigned to the asymmetric N–C–N stretching mode of adsorbed urea [14]. The absorptions at 1584 and 1610 cm^{-1} are both due to the NH_2 bending mode of adsorbed urea [14]. The bands at 1650 and 1712 cm^{-1} (both C=O stretching mode) can be assigned to urea adsorbed at different sites or in different coordination environments in NaY zeolite [14]. Some additional bands in the spectral region of 3100–3800 cm^{-1} due to O–H/N–H stretching are also seen (not shown). The general features of the FTIR spectrum of nanocrystalline NaY zeolite with adsorbed urea (not shown) are similar to those of commercial NaY zeolite, except for increased spectral broadening of the peaks in nanocrystalline NaY. This broadening has been previously attributed to increased site heterogeneity for nanocrystalline zeolite samples [32].

The NaY sample with adsorbed urea was then exposed to 0.5 Torr pressure of NO_2 at room temperature and equilibrated for 30 min. The changes in the FTIR spectra of the NaY sample upon exposure and equlibrium with NO_2 are clearly seen in the difference spectra shown in Fig. 2. Each difference spectrum was obtained by subtracting the spectrum of NaY zeolite before adsorbing NO_2 from the corresponding spectrum after the adsorption equilibrium. As shown in the difference FTIR spectrum of commercial NaY

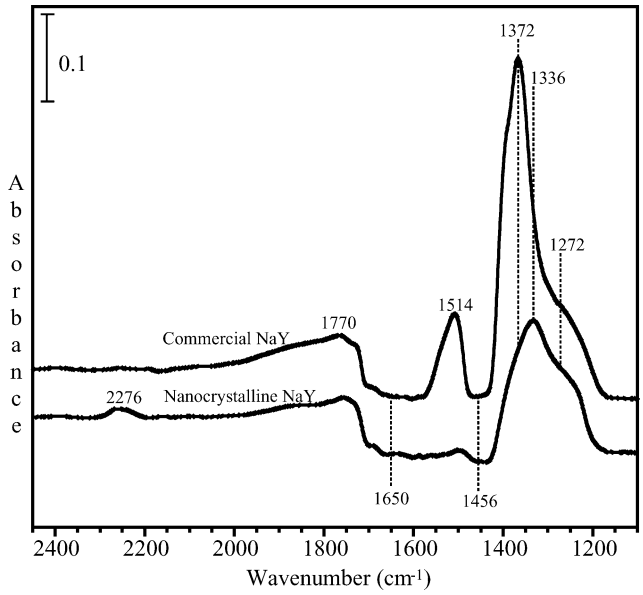

Fig. 2. Difference FTIR spectra of nanocrystalline NaY with adsorbed urea and commercial NaY zeolite with adsorbed urea following adsorption of 0.5 Torr NO_2 at $T = 298$ K. The spectra use the corresponding NaY zeolite with adsorbed urea prior to NO_2 adsorption as a background. In addition, gas-phase absorptions have been subtracted from each of the FTIR spectra.

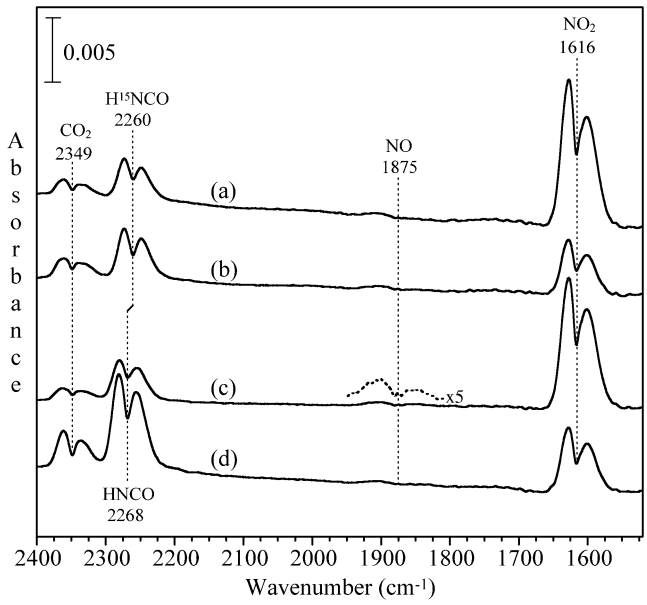

Fig. 3. The FTIR spectra of the gas phase upon adsorption of NO_2 in (a) commercial NaY zeolite with adsorbed ^{15}N-urea, (b) nanocrystalline NaY zeolite with adsorbed ^{15}N-urea, (c) commercial NaY zeolite with adsorbed unlabeled urea, and (d) nanocrystalline NaY zeolite with adsorbed unlabeled urea. All spectra were recorded at $T = 298$ K after adsorption equilibrium. The NO signal at ~1875 cm^{-1} has been increased by a factor of 5 in the spectrum labeled (c) and is representative of the NO signal intensity in all of the spectra in this figure.

zeolite (Fig. 2), several absorption bands appeared at 1272, 1372, 1514, and 1770 cm^{-1}. The absorption bands at 1272 and 1372 cm^{-1} are attributed to the formation of nitrite and nitrate on Na^+ sites, respectively [24,31,32,40,41]. The appearance of two absorption peaks at 1514 cm^{-1} ($\nu_{CN} + \delta_{NH}$) and 1770 cm^{-1} (ν_{CO}) indicate the formation of a surface species with a linear imido structure [e.g., –(C=O)–NH–(C=O)–] [12]. A simultaneous loss in intensity of the bands around 1456 and 1650 cm^{-1} was observed, indicating that adsorbed urea reacted with NO_2 (or surface species generated in NO_2 adsorption).

The difference FTIR spectrum of nanocrystalline NaY with adsorbed urea after being exposed to NO_2 is shown in Fig. 2 (bottom spectrum). Similar to the commercial NaY zeolite, the formation of nitrite (1272 cm^{-1}) and disappearance of adsorbed urea (1456 and 1650 cm^{-1}) were observed for nanocrystalline NaY zeolite. However, several differences in the spectra of nanocrystalline NaY zeolite and commercial NaY zeolite were observed. For example, formation of the surface species with the linear imido structure (1514 and 1770 cm^{-1}) occurred to a much lesser extent in nanocrystalline NaY (Fig. 2). Furthermore, NO_2 adsorption in nanocrystalline NaY zeolite resulted in the formation of nitrate adsorbed on external (vide infra) EFAL sites (1336 cm^{-1}) [31,32], as well as nitrate on internal Na^+ sites (1372 cm^{-1}). Finally, the formation of isocyanic acid (HNCO) adsorbed on EFAL sites is observed in nanocrystalline NaY zeolite, as indicated by a broad absorption band around 2276 cm^{-1} [27,31,32]. In NO_2 adsorption at room temperature, the formation of surface-adsorbed isocyanic acid is not appreciable in commercial NaY zeolite (Fig. 2). Previous studies of pyridine adsorption coupled with IR analysis indicate that EFAL sites are located on the external surface of nanocrystalline NaY zeolite and are not present to any great extent in the commercial NaY sample because of its low external surface area [30–32].

Unlabeled urea and ^{15}N-labeled urea were used in SCR reactions over both nanocrystalline NaY and commercial NaY zeolite. Compared with the FTIR spectrum of NaY zeolite with unlabeled urea, several differences were observed when ^{15}N-urea solution was mixed with the zeolite sample. For example, the absorption band for adsorbed $H^{15}NCO$ shifted from 2276 to 2258 cm^{-1} when nanocrystalline NaY with adsorbed ^{15}N-urea was exposed to NO_2 at room temperature (not shown). A similar isotopic shift was also observed for gas-phase HNCO. The FTIR spectra of the gas phase after NO_2 adsorption in commercial and nanocrystalline NaY zeolite with unlabeled urea and ^{15}N-urea are shown in Fig. 3. Gas-phase NO_2 (1616 cm^{-1}), NO (1875 cm^{-1}), HNCO (2268 cm^{-1}), and CO_2 (2349 cm^{-1}) were observed when NaY zeolite with adsorbed urea was exposed to NO_2 at room temperature [27,31,42]. For gas-phase HNCO, an isotopic shift of 8 cm^{-1} was observed after substituting ^{15}N for ^{14}N [27]. The complete list of isotopic shifts for nitrogen-containing gas phase and adsorbed species is given in Table 1 and is discussed in detail later in this paper. In the spectra shown in Fig. 3, the absorption band for gas-phase NO_2 over nanocrystalline NaY zeolite is less intense than that over commercial NaY, indicating that more NO_2 was adsorbed/reacted with nanocrystalline NaY zeolite relative to commercial NaY. This finding is consistent with our

Table 1
List of vibrational frequencies of nitrogen-containing gas-phase and adsorbed species which showed an isotopic shift upon substitution of ^{15}N for ^{14}N in the adsorbed urea ($(NH_2)_2CO$) precursor

	Product	Assignment	$\nu(^{14}N)$	$\nu(^{15}N)$	$\Delta\nu$[a]	$\nu(^{14}N)/\nu(^{15}N)$
Gas phase	HNCO	ν_{NCO}	2268	2260	8	1.004
	N_2O	ν_{NN}	2224	2201	23	1.010
	N_2O	ν_{NO}	1285	1270	15	1.012
	NH_3	δ_{NH_3}	965	960	5	1.005
Adsorbed in nanocrystalline NaY	HNCO	ν_{NCO}	2276	2258	18	1.008
	OCN^-	ν_{NC}	2169	2153	16	1.007
	$(NH_2)_2CO$	ν_{CNH}	1527	1522	5	1.003
	$(NH_2)_2CO$	ν_{CNH}	1271	1266	5	1.004
Adsorbed in commercial NaY	HNCO	ν_{NCO}	2282	2250	32	1.014
	OCN^-	ν_{NC}	2175	2159	16	1.007
	$(NH_2CO)_2NH$	ν_{CO}	1759	1751	8	1.005
	$(HNCO)_3$	ν_{CO}	1735	1727	8	1.005

[a] $\Delta\nu = \nu(^{14}N) - \nu(^{15}N)$.

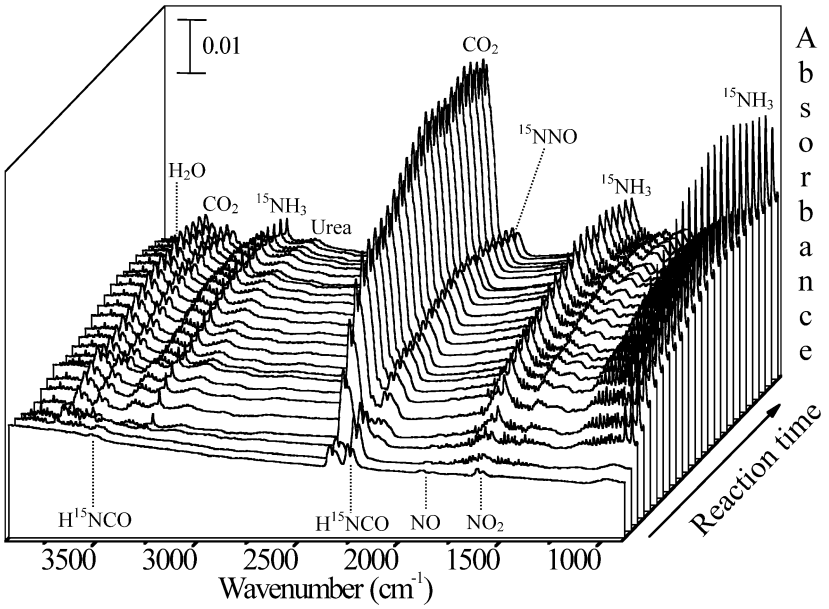

Fig. 4. FTIR spectra of the gas phase as a function of reaction time in ^{15}N-urea SCR of NO_2 over nanocrystalline NaY zeolite in the presence of oxygen. The spectra shown were recorded at $T = 473$ K and at t (reaction time) = 0, 1, 2, 3, 4, 5, 6, 7, 8, 9, 10, 11, 12, 13, 14, 15, 16, 17, 18, 19, 21, 23, 25, 27, 30 min, respectively. The blank grid is used as a reference.

previous observation that nanocrystalline NaY zeolite has a greater adsorption capacity for NO_2 than commercial NaY zeolite [30,32].

3.2. Urea-SCR of NO_2 in NaY zeolite at $T = 473$ K: Gas phase products

An excess amount of O_2 was introduced into the FTIR cell after the NaY zeolite sample was equilibrated with NO_2 for 30 min at room temperature. Urea-SCR of NO_2 was then carried out at $T = 473$ K. A control experiment was done by heating the commercial NaY zeolite with adsorbed urea at $T = 473$ K in the presence of oxygen.

Fig. 4 shows the FTIR spectra of gas-phase species formed during the first 30 min of ^{15}N-urea SCR over nanocrystalline NaY zeolite at $T = 473$ K. In the beginning of the SCR reaction ($t = 0$), gas-phase NO_2, NO, $H^{15}NCO$, CO_2, and a small amount of H_2O were observed in the FTIR spectrum. At $t = 1$ min, more H_2O and $H^{15}NCO$ appeared in the gas phase, as shown by the spectra (Fig. 4). Gas-phase $H^{15}NCO$ decayed quickly after $t = 2$ min. Several other changes in gas phase composition can be seen in these time course experiments, including the rapid production of $^{15}NH_3$ (927, 960, 1623, and 3331 cm^{-1}) and CO_2 at $t = 2$ min. Gas-phase ^{15}N-urea appeared and is identified by several characteristic absorptions, including three broad bands between 3100 and 3520 cm^{-1} and several absorptions between 1290 and 1720 cm^{-1} in the FTIR spectra shown in Fig. 4. Furthermore, gas-phase NO_2 disappeared quickly relative to NO. ^{15}NNO (2201 and 1270 cm^{-1}) ap-

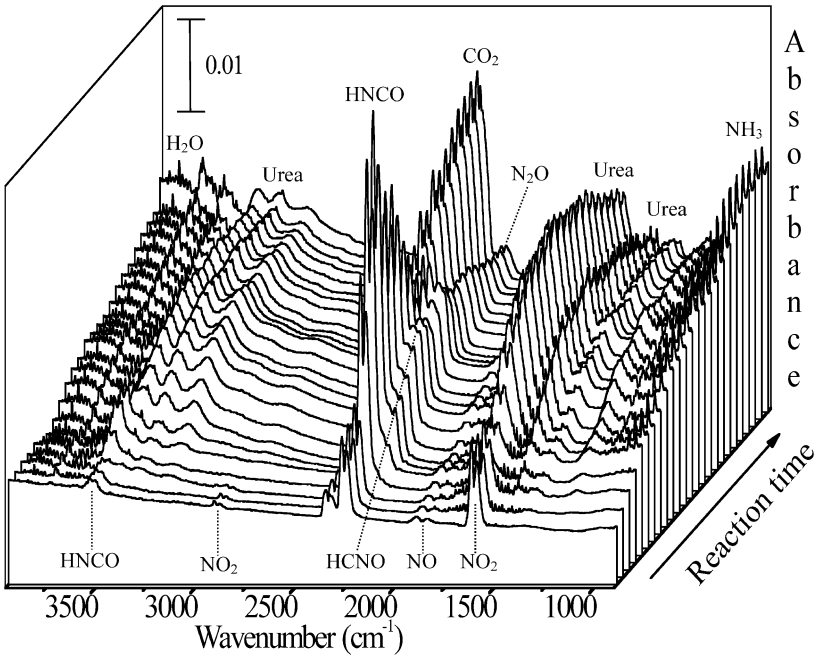

Fig. 5. FTIR spectra of the gas phase as a function of reaction time in urea-SCR of NO_2 over commercial NaY zeolite in the presence of oxygen. The spectra shown were recorded at $T = 473$ K and at t (reaction time) = 0, 1, 2, 3, 4, 5, 6, 7, 8, 10, 12, 14, 16, 18, 20, 25, 30, 35, 40, 50, 60, 70, 80, 90, 120 min, respectively. The blank grid is used as a reference.

peared in these spectra as the only isomer of N_2O (Table 1) [43]. Other isomers of N_2O, such as $N^{15}NO$ and $^{15}N_2O$, have different absorption frequencies (2178/1280 cm^{-1} for $N^{15}NO$ and 2155/1265 cm^{-1} for $^{15}N_2O$) and were not detected in our experiments [43]. The formation of ^{15}NNO in the gas phase indicates that N–N bond formation at 473 K involved a ^{15}N-atom originating from urea and a ^{14}N-atom originating from NO_2 and that the N=O bond in NO_2 remained intact during the formation of ^{15}NNO. There was no significant change in the gas phase after 30 min of SCR reactions over nanocrystalline NaY zeolite.

Compared with the SCR reaction in nanocrystalline NaY zeolite, the urea-SCR of NO_2 in commercial NaY zeolite was much slower. The FTIR spectra of the gas phase species present during the 2 h of urea-SCR over commercial NaY zeolite are shown in Fig. 5. In urea-SCR using commercial NaY catalyst, NO_2 disappeared quickly, but NO persisted in the gas phase during the 2 h reaction period. The concentration of HNCO reached a maximum at $t = 5$ min, and HNCO remained detectable in the IR cell for at least 60 min during the SCR reaction process (Fig. 5). There was an induction period (∼3 min) for the production of NH_3 and CO_2 that did not appear in the gas phase with significant concentrations until $t = 4$ min (Fig. 5). N_2O appeared as one of the final products in the gas-phase [31,32]. A gas phase species with an absorption around ∼2185 cm^{-1} was present in the FTIR spectra from $t = 4$ to 10 min. Because another absorption band at 1255 cm^{-1} was also observed (not labeled), this species is assigned to formonitrile oxide (HCNO) [42,44,45]. Further supporting this assignment is the fact that HCNO (2190 and 1255 cm^{-1}) was produced in the presence of large amounts of HNCO during the thermal decomposition of urea at $T = 473$ K in commercial NaY zeolite (data not shown).

The time course concentrations of the gases in the IR cell can be determined from the integrated absorbance of the corresponding IR absorptions using calibrated extinction coefficients, as described in previous work [31,32]. The time course concentrations of gas-phase NH_3, CO_2, and H_2O in urea-SCR of NO_2 are shown in Fig. 6. The time course concentrations for the urea thermal decomposition over commercial NaY zeolite are also included in Fig. 6. It should be noted that the concentration of gas-phase H_2O rapidly increased to a maximum at $t = 2$ min in urea-SCR of NO_2 over nanocrystalline NaY zeolite (Fig. 6c). The concentration of gas-phase H_2O then decreased sharply until a minimum was reached at approximately $t = 15$ min and started increasing again thereafter. Most likely, strongly adsorbed water that remained in nanocrystalline NaY zeolite was released initially upon heating to $T = 473$ K [31], followed by the consumption and production of H_2O in SCR reactions [12].

The time course concentrations of NO and N_2O in the gas phase are shown in Fig. 7. In urea-SCR of NO_2 over nanocrystalline NaY zeolite, the concentration of NO decreased monotonically and gas-phase NO disappeared completely around $t = 40$ min (Fig. 7a). When commercial NaY zeolite was used as the SCR catalyst, the NO concentration initially increased until it reached a maximum level and decreased slowly thereafter. The time course concentration of N_2O demonstrates that N_2O was produced more quickly and in much higher concentration in nanocrystalline NaY zeolite than in commercial NaY zeolite (Fig. 7b).

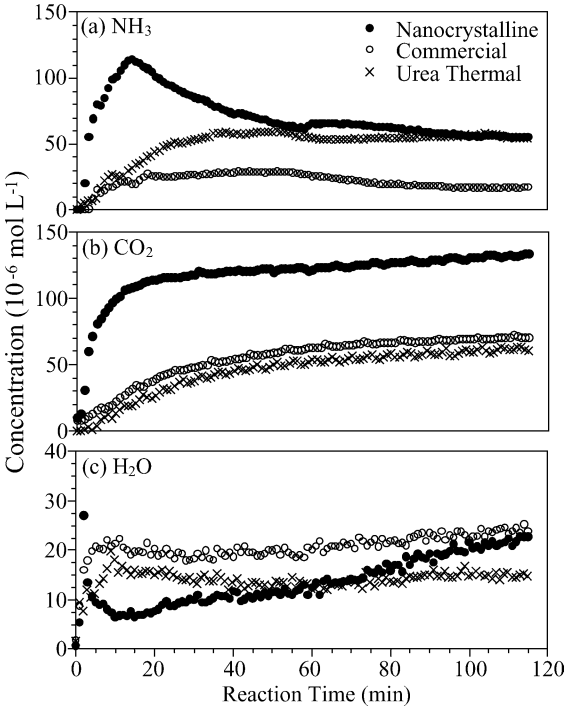

Fig. 6. Evolution of gas-phase (a) NH_3, (b) CO_2 and (c) H_2O during urea-SCR of NO_2 in nanocrystalline NaY zeolite (●), urea-SCR of NO_2 in commercial NaY zeolite (○) and thermal decomposition of urea in commercial NaY zeolite (×) at $T = 473$ K in the presence of oxygen.

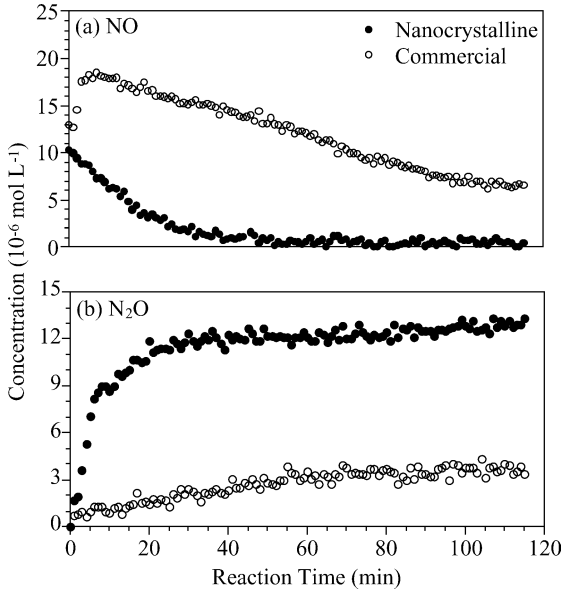

Fig. 7. Evolution of gas-phase (a) NO and (b) N_2O during urea-SCR of NO_2 in nanocrystalline NaY zeolite (●) and in commercial NaY zeolite (○) at $T = 473$ K in the presence of oxygen.

The initial rates for formation of gas-phase NH_3, CO_2, and N_2O and loss of gas-phase NO can be obtained by linear fitting of the concentrations of individual gas-phase species in the beginning of the reactions, as listed in Table 2. In urea-SCR of NO_2 over nanocrystalline NaY zeolite, the initial rate of NH_3 formation is slightly higher than the initial rate of CO_2 formation. In the thermal reaction of urea over commercial NaY zeolite, the ratio of NH_3 formation rate to CO_2 formation rate is close to 2:1, which matches the fact that 1 mol of urea thermally decomposes into 2 mol of NH_3 and 1 mol of CO_2 (reactions (1) and (2)). Furthermore, the initial rates for NH_3 and CO_2 formation are much higher in nanocrystalline NaY than in commercial NaY. Table 2 also includes the initial rates of N_2O formation and NO loss. It can be concluded from the data listed in Table 2 that urea SCR of NO_2 occurred more quickly in nanocrystalline NaY than in commercial NaY zeolite.

Table 2
Rates for formation of gas-phase NH_3, CO_2 and N_2O and loss of gas-phase NO in the first 10 min during urea-SCR of NO_2 and thermal decomposition of urea at $T = 473$ K

Catalyst	Initial rate (μmol/(L min))			
	NH_3	CO_2	NO	N_2O
Nanocrystalline NaY	10.3	8.9	−0.4	1.1
Commercial NaY	2.4	1.5	−0.2[a]	0.1
Commercial NaY[b]	3.0	1.6	–	–

[a] The initial rate of NO loss during the urea-SCR of NO_2 over commercial NaY zeolite was measured from $t = 9$ to 18 min.
[b] Thermal decomposition of urea in the presence of O_2.

Table 3
Gas-phase product distribution after urea-SCR of NO_2 and thermal reaction of urea at $T = 473$ K for 2 h in 7 mg NaY zeolite. The loadings of NO_2, urea and O_2 are 70 ± 5, 170 ± 20, and 550 ± 20 μmol/L in the IR cell with a volume of 0.32 ± 0.01 L, respectively

Catalyst	Concentration (μmol/L)[a]			
	NH_3	CO_2	NO	N_2O
Nanocrystalline NaY	56	138	0	12
Commercial NaY	17	74	7	4
Commercial NaY[b]	53	69	–	–

[a] The concentration of gas-phase NH_3 was measured at $T = 473$ K, the concentrations of gas-phase CO_2, NO and N_2O were measured at $T = 298$ K.
[b] Thermal reaction of urea in the absence of NO_2.

Table 3 summarizes the product distribution in the gas phase after urea-SCR of NO_2 and thermal reaction of urea. The concentrations of NH_3 and CO_2 after SCR reaction are much higher in nanocrystalline NaY zeolite than in commercial NaY zeolite. In addition, urea-SCR of NO_2 over nanocrystalline NaY zeolite resulted in 100% NO_x (NO_2 and NO) conversion and higher selectivity toward N_2O formation relative to commercial NaY zeolite. Based on mass balance for nitrogen, more than 80% of NO_2 was converted into N_2 in urea-SCR over nanocrystalline NaY zeolite at $T = 473$ K (Table 3).

3.3. *Urea-SCR of NO_2 in NaY zeolite at $T = 473$ K: adsorbed products*

Besides kinetics studies, FTIR analysis of surface adsorbed intermediates or products can improve understanding of the mechanism behind urea-SCR of NO_2 [31,32]. Differ-

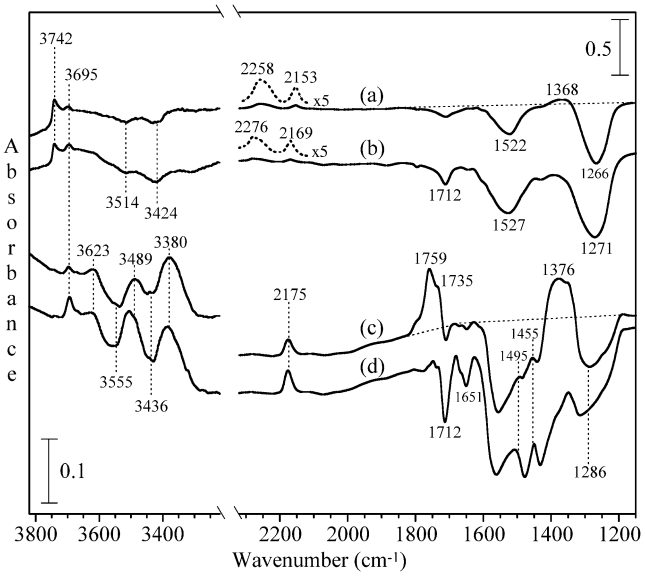

Fig. 8. Difference FTIR spectra of zeolite samples following (a) ^{15}N-urea-SCR of NO_2 in nanocrystalline NaY for 30 min, (b) urea SCR of NO_2 in nanocrystalline NaY for 2 h, (c) urea-SCR of NO_2 in commercial NaY for 2 h and (d) thermal decomposition of urea in commercial NaY for 2 h at $T = 473$ (from top to bottom) in the presence of oxygen. The spectra were recorded at $T = 298$ K. All spectra shown use the corresponding NaY zeolite with adsorbed urea prior to NO_2 adsorption as a background. In addition, gas-phase absorptions have been subtracted from each of the FTIR spectra shown.

ence FTIR spectra of nanocrystalline NaY and commercial NaY zeolite after urea-SCR of NO_2 are shown in Fig. 8. This figure also shows the difference FTIR spectra of nanocrystalline NaY zeolite after ^{15}N-urea SCR of NO_2 and commercial NaY zeolite after thermal reaction of urea. The zeolite samples were cooled back to room temperature before the spectra were recorded. It was observed that most gas phase NH_3, H_2O, and urea disappeared from the gas phase after the zeolites were cooled back to room temperature, because of adsorption in the zeolite samples.

In urea-SCR of NO_2 over nanocrystalline NaY zeolite, the formation of adsorbed HNCO and OCN^- can be identified by the absorption bands at 2276 cm^{-1} [27,31,32] and 2169 cm^{-1} [27,46], respectively, in the FTIR spectra shown in Fig. 8b. The loss of adsorbed urea, characterized by the negative absorptions at 1271, 1527, and 1712 cm^{-1} (ν_{CO}) and 3424 and 3514 cm^{-1} (both ν_{NH}), can also be seen in the spectra. The absorption band at 1527 cm^{-1} is assigned to the CNH bend-stretch mode, in which the nitrogen and hydrogen move in opposite directions relative to the carbon, whereas the absorption band at 1271 cm^{-1} is assigned to the CNH open-stretch mode, in which N and H atoms move in the same direction relative to the carbon [47]. In addition, the recovery of silanol groups (3742 cm^{-1}) and OH groups attached to Na^+ (3695 cm^{-1}) are evident in the spectrum of nanocrystalline NaY zeolite shown in Fig. 8b [30–32]. This indicates that adsorption and SCR reactions occurred to a significant extent on the external surface, because silanol groups are present mainly on the external surface of the nanocrystalline NaY zeolite [30,32].

The difference FTIR spectrum of nanocrystalline NaY seen after ^{15}N-urea SCR of NO_2 for 30 min (Fig. 8a) is similar to that seen after urea-SCR for 2 h (Fig. 8b). The formation of adsorbed H^{15}NCO (2258 cm^{-1}) and O$C^{15}N^-$ (2153 cm^{-1}), as well as the loss of adsorbed ^{15}N-urea (1522 and 1266 cm^{-1}), are apparent in this spectrum. The isotopic shifts for these nitrogen-containing species are apparent in the spectrum and are listed in Table 1. In the spectrum shown in Fig. 8a, a dotted baseline is drawn in the range 1200–1800 cm^{-1}, revealing that a small amount of nitrate remained in nanocrystalline NaY zeolite after 30 min of SCR reaction at $T = 473$ K.

When commercial NaY zeolite was used as the SCR catalyst, a loss of adsorbed urea was observed, as indicated by the negative absorption bands at 1286 cm^{-1} (ν_{CNH}), 1651 and 1712 cm^{-1} (both $\nu_{C=O}$), and 3436 and 3555 cm^{-1} (both ν_{NH}) in the spectrum of commercial NaY zeolite after urea-SCR reactions (Fig. 8c). The other CNH vibration that should fall between 1400 and 1600 cm^{-1} may be less pronounced in the spectrum, because of the formation of two absorption bands at 1455 and 1495 cm^{-1} (Fig. 8c). The two absorption bands at 1455 and 1495 cm^{-1} are assigned to the bending mode of adsorbed ammonium ion and stretching mode of surface species containing imine groups (C=NH), respectively [12]. In the spectrum shown in Fig. 8c, the corrected baseline (dotted line) in the range 1200–1800 cm^{-1} clearly demonstrates the formation of adsorbed biuret (1759 cm^{-1}) [12] and cyanuric acid (1735 cm^{-1}) [48] in commercial NaY zeolite after SCR reactions. Furthermore, surface OCN^- (2175 cm^{-1}) [46] and nitrate (1376 cm^{-1}) were observed after urea-SCR of NO_2 for 2 h in commercial NaY zeolite. In the OH/NH stretching region (Fig. 8c), the absorptions in the spectrum of commercial NaY zeolite indicate the formation of OH group on Na^+ (3695 cm^{-1}), surface-adsorbed H_2O (3623 cm^{-1}), and NH-containing species (3220, 3380, 3489 cm^{-1}), as well as the loss of adsorbed urea (3436 and 3555 cm^{-1}). The FTIR spectrum of commercial NaY zeolite after thermal reaction of urea is almost the same as that after urea-SCR of NO_2, except that nitrate, biuret, and cyanuric acid formation is not observed in the thermal decomposition of urea (Fig. 8d).

The comparison between the difference FTIR spectra of the zeolite samples after urea-SCR of NO_2 for 2 h indicates that greater nitrate conversion was achieved in nanocrystalline NaY zeolite than in commercial NaY zeolite. This finding is consistent with the fact that urea-SCR of NO_2 is much slower in commercial NaY than in nanocrystalline NaY, as mentioned earlier (see Table 2). Furthermore, undesired surface products (biuret and cyanuric acid) were observed in commercial NaY zeolite, but not in nanocrystalline NaY zeolite, after urea-SCR of NO_2.

The assignments of absorption bands in FTIR spectra shown in Fig. 8 are further supported by isotopic studies (Table 1). The absorption frequencies for HNCO and OCN^-

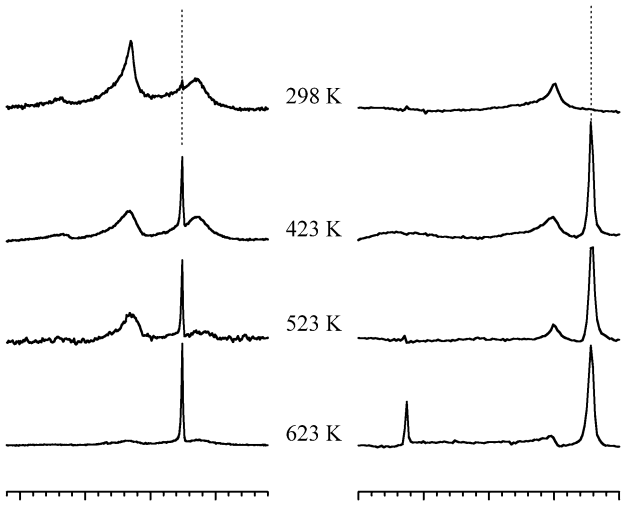

Fig. 9. ^{13}C single pulse (a) and ^{15}N single pulse (b) MAS NMR of labeled urea (^{13}C and ^{15}N), NO and O_2 adsorbed in nanocrystalline NaY at $T = 298$, 423, 523 and 623 K (from top to bottom). Spectra were acquired at room temperature after heating to the desired temperatures. Numbers of scans taken for ^{13}C and ^{15}N spectra were 20000 and 10000, respectively. Line broadening = 50 Hz.

in nanocrystalline NaY zeolite are different from those in commercial NaY zeolite. In nanocrystalline NaY, HNCO (2276 cm^{-1}) and OCN^- (2169 cm^{-1}) are most likely adsorbed on EFAL sites [31,32]. In commercial NaY zeolite, OCN^- is characterized by the relatively intense absorption band at 2175 cm^{-1} in the FTIR spectrum shown in Fig. 8c and is most likely attached to Na^+ sites [27]. In nanocrystalline NaY zeolite, the isotopic shift for the CNH vibration mode of adsorbed urea (5 cm^{-1}) is exactly the same as that for the NH_3 deformation mode of gas-phase NH_3. This suggests that urea was adsorbed in nanocrystalline NaY zeolite in such a way that at least one NH_2 group remained almost unperturbed [14]. In commercial NaY zeolite, the isotopic shift for the C=O stretching mode of adsorbed biuret and cyanuric acid (8 cm^{-1}) is the same as that for the NCO stretching mode of gas-phase HNCO. This may be due to the configuration exchange

–(C=O)–NH– ↔ –C(OH)=N–

in adsorbed biuret and cyanuric acid in commercial NaY zeolite.

3.4. Complementary solid-state NMR (^{13}C and ^{15}N) spectra of labeled urea, NO, and O_2 in nanocrystalline NaY

The ^{13}C MAS NMR spectra for urea (^{13}C- and ^{15}N-labeled), NO, and O_2 in nanocrystalline NaY, shown in Fig. 9a, has a ^{13}C peak at 165 ppm before heating. This peak is assigned to the carbonyl group of adsorbed urea [16]. After heating to $T = 423$ K, a narrow intense peak is present at 125 ppm that can be assigned to CO_2. After heating to $T = 623$ K, there is a substantial increase in peak intensity for CO_2 at 125 ppm, whereas the peak at 165 ppm is no longer present. Fig. 9b shows the ^{15}N MAS NMR of urea (^{13}C- and ^{15}N-labeled), NO, and O_2 in nanocrystalline NaY. Before heating, the ^{15}N peak at −301 ppm is present and is assigned to the adsorbed urea. After heating to $T = 423$ K, ammonia is produced, as indicated by the peak at −356 ppm. After heating to $T = 523$ K, a peak at −74 ppm is present and is assigned to N_2. After heating to $T = 623$ K, a substantial increase in the N_2 peak and loss of intensity for the ammonia peak are seen.

The solid-state NMR spectra were acquired under conditions of thermal equilibrium because of the long time periods needed for signal averaging. In the presence of oxygen, the adsorption of NO in zeolite Y occurs in a similar manner as the adsorption of NO_2 [24], because of the oxidation of NO into NO_2 [40]. Thus these NMR results can be readily compared with the FTIR data in this study. The NMR results are also consistent with the FTIR results, in that urea thermally decomposes to form NH_3 and CO_2 at elevated temperatures in the presence of NO and O_2. The most important aspect of the NMR results is the observation of N_2 formation, which cannot be observed directly by FTIR spectroscopy.

4. Discussion

4.1. Reactions between gas-phase NO_2 and adsorbed urea in NaY zeolite at $T = 298$ K

The adsorption of NO_2 in zeolite Y has been described in detail in the literature [24,27,31,32,40,41]. In this study, NO_2 reacted with adsorbed water by reaction (3) or (4) in NaY zeolite, because a considerable amount of water remained in the zeolite after the zeolite samples were evacuated at room temperature [32,41]:

$$2NO_2 + H_2O \rightarrow HNO_3 + HONO, \quad (3)$$

$$3NO_2 + H_2O \rightarrow 2HNO_3 + NO. \quad (4)$$

The nitric acid and nitrous acid further deprotonate and adsorb on surface cationic sites to form surface nitrate and nitrite. This explains the formation of surface nitrate, nitrite (Fig. 2), and gas-phase NO after NO_2 adsorption in NaY zeolite (Fig. 3). Nitrate formation on EFAL sites in nanocrystalline NaY zeolite was also observed (Fig. 2). In nanocrystalline NaY zeolite, NO_2 adsorption occurs in part on cationic sites of EFAL species (M^{n+}–O^-), according to reaction (5) [24,31,32]:

$$M^{n+}\text{–}O^- + NO_2 \rightarrow M^{n+}\text{–}NO_3{}^-. \quad (5)$$

The formation of NO, HNCO, and a small amount of CO_2 and H_2O was observed when NO_2 was adsorbed in NaY zeolite with adsorbed urea at room temperature (Figs. 3–5). Isotopic labeling shows that the N-atom in HNCO originates from urea (Fig. 4). The loss of adsorbed urea was observed as well upon the adsorption of NO_2 (Fig. 3). Because the decomposition of urea into HNCO and NH_3 is not significant at room temperature [12], HNCO most likely formed in the

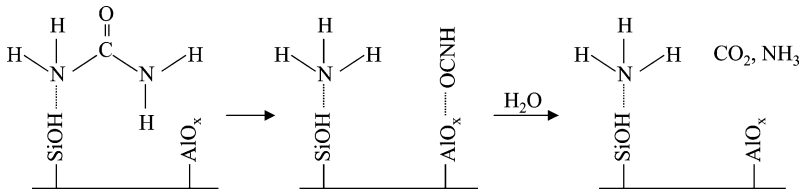

Scheme 1. Thermal decomposition of urea on silanol (SiOH) and EFAL (AlO_x) sites in nanocrystalline NaY zeolite.

reactions between adsorbed urea and HNO_3 (reaction (6)) [14]. The reaction between the adsorbed urea and HONO can lead to the formation of CO_2 and H_2O at room temperature:

$$(NH_2)_2CO + HNO_3 \rightarrow HNCO + NH_4NO_3, \quad (6)$$

$$(NH_2)_2CO + 2HONO \rightarrow 2N_2 + CO_2 + 3H_2O. \quad (7)$$

NH_4NO_3 can thermally decompose into $N_2O + 2H_2O$, providing a minor route for N–N bond formation in urea SCR of NO_2 in NaY zeolite [26,49]. Reaction (7) is used in destroying excess nitrous acid in diazotization [50].

When commercial NaY zeolite was exposed to NO_2 at room temperature, surface species with a linear imido structure, such as biuret, appeared. This surface species is most likely generated in the reactions between HNCO and adsorbed urea (Fig. 2). Amide carbonyls of biuret and triuret have characteristic absorption bands ~1750–1770 cm^{-1} [12]. Biuret can be produced via reaction (8) [50],

$$NH_2–CO–NH_2 + HNCO \rightarrow NH_2–CO–NH–CO–NH_2. \quad (8)$$

The above analysis suggests that EFAL species in nanocrystalline NaY zeolite provide additional surface sites for NO_2 adsorption and its further reactions at room temperature. Previous studies have shown that EFAL sites on the external surface of nanocrystalline NaY zeolite are important for the formation of reactive nitrate and for the subsequent SCR reactions [32]. In this study, EFAL sites in nanocrystalline NaY zeolite also provide important reactive surface sites for HNCO and inhibit the formation of undesired products, such as biuret or triuret.

4.2. Insights into urea-SCR of NO_2 in nanocrystalline NaY zeolite at $T = 473$ K

The FTIR spectra of the gas phase shown in Fig. 4 demonstrate that thermal decomposition of urea occurred at $T = 473$ K in nanocrystalline NaY zeolite. As described previously, gas-phase HNCO was produced initially and decayed rapidly after $t = 2$ min (Fig. 4). The initial change in H_2O concentration (Fig. 6c) was similar to that of HNCO. At $t = 2$ min, the concentration of NH_3 in gas phase began to increase sharply (Fig. 6a). According to reaction (1), the first step in thermal decomposition of urea produced equal amounts of HNCO and NH_3. This suggests that most NH_3 produced in thermal decomposition of urea remained in the nanocrystalline NaY zeolite. In addition, the concentrations of NH_3 and CO_2 in the gas phase increased sharply after $t = 2$ min (Figs. 6a and 6b). The initial formation rates of gas-phase NH_3 and CO_2 shown in Table 2 correlate well with the stoichiometry shown by reaction (2), in which 1 mol of HNCO hydrolyzes to form 1 mol of NH_3 and 1 mol of CO_2. Most likely, NH_3 formed in hydrolysis of HNCO in the zeolite enters the gas phase immediately at $T = 473$ K.

Moreover, both the loss of adsorbed urea and regeneration of surface silanol groups were observed in nanocrystalline NaY zeolite after urea-SCR of NO_2 (Fig. 8). The absorption frequencies for the urea adsorbed in nanocrystalline NaY are different from those in commercial NaY, which contains few silanol groups (Table 1) [30,32]. We can conclude that the adsorption and thermal decomposition of urea in nanocrystalline NaY zeolite involved the silanol groups on the external surface. Finally, HNCO produced in thermal decomposition of urea adsorbed and most likely hydrolyzed on EFAL sites in nanocrystalline NaY zeolite. This finding is supported by the fact that HNCO adsorbed on EFAL sites was observed before (Fig. 2) and after urea-SCR of NO_2 (Fig. 8) in nanocrystalline NaY zeolite.

Scheme 1 describes the adsorption and thermal decomposition of urea on the external surface of nanocrystalline NaY zeolite before N–N bond formation. Initially, urea adsorbed in nanocrystalline NaY zeolite by hydrogen bonding to silanol groups on the external surface through one N atom, leaving the other NH_2 almost unperturbed [14]. This is consistent with the isotopic studies showing that the isotopic shift for the CNH vibration mode is the same as the isotopic shift for the NH_3 deformation mode of gas-phase NH_3 (Table 1). At elevated temperature ($T = 473$ K), urea decomposed into HNCO and NH_3. While NH_3 remained on the silanol groups of nanocrystalline NaY zeolite via hydrogen bonding, HNCO adsorbed on EFAL sites and continued to hydrolyze and produce CO_2 and additional NH_3. The loss of silanol groups was observed when NH_3 was adsorbed in clean nanocrystalline NaY at room temperature and at $T = 473$ K.

In urea-SCR of NO_2 over nanocrystalline NaY zeolite, isotopic studies indicate that the N–N bond formation involved both an N atom originating from the adsorbed urea and an N atom originating from gas-phase NO_2 (Fig. 4). NH_3 produced in thermal decomposition of urea is the actual reducing reagent in NO_x reduction [2,12–14]. It has been suggested that OH groups and surface acid sites on the catalyst surface can coordinate with and further activate NH_3 [2,8].

Although the concentration of gas-phase NO decreased monotonically in urea-SCR of NO_2 over nanocrystalline

NaY zeolite (Fig. 7a), further analysis indicates that both the formation and consumption of NO occurred. NO is the major gas-phase product in thermal reactions of nitrate and nitrite in nanocrystalline NaY zeolite at 473 K [31,32]. In the present work, the initial rate of N_2O formation is much greater than the initial rate of NO loss in urea-SCR of NO_2 over nanocrystalline NaY zeolite (Table 2). The actual initial rate for N–N bond formation should be even greater, because >80% of the NO_2 was converted to N_2 in urea-SCR of NO_2 over nanocrystalline NaY zeolite. In urea-SCR of NO_2 over commercial NaY zeolite, the concentration of NO initially increased, then decreased after 9 min (Fig. 7a). A similar time course concentration of NO was found in propylene-SCR of NO_2 in nanocrystalline NaY [31].

It has been proposed that in NH_3-SCR reactions using transition metal zeolite catalysts, NH_3 adsorbed on surface acid sites reacts directly with gas-phase NO to form N_2 and H_2O [2,20]. Recent studies by Yeom et al. [25,26] have demonstrated that NO participates in a number of reactions in the NO_x reduction network over BaNaY zeolite. Ammonium nitrate is an SCR intermediate that can thermally decompose to form N_2O or can react with NO to produce ammonium nitrite [25]. In micrometer-sized BaNaY, thermal decomposition of ammonium nitrate yielded N_2O at 585 K [26]. A significant amount of N_2O was produced in urea-SCR of NO_2 over nanocrystalline NaY at 473 K (Table 3; Fig. 7b), suggesting that ammonium nitrate decomposition may occur at a lower temperature on nanocrystalline NaY. But ammonium nitrate absorption around 3270, 1460, and 1350 cm^{-1} was not evident in the FTIR spectra presented in this study [51]. Although this finding suggests that no ammonium nitrate is present, another possibility is that the ammonium bands were obscured in the FTIR spectrum because of spectral congestion in these regions due to broad absorption bands from other adsorbed species.

Ammonium nitrite is an important SCR intermediate that decomposes efficiently near 373 K to N_2 and H_2O on Y zeolites [25–27]. The formation of N_2 and loss of NO observed in the present study are consistent with the formation of ammonium nitrite and its subsequent decomposition to N_2. However, ammonium nitrite bands are not apparent in the FTIR spectra presented in this study. Therefore, because ammonium nitrate and ammonium nitrite were not directly observed in our experiments, a definite mechanistic pathway cannot be elucidated at this time. Further studies are needed to investigate ammonium nitrate (nitrite) reactivity on nanocrystalline NaY.

4.3. Origin of size effect in urea-SCR of NO_2 over NaY zeolite

Reducing the zeolite crystal size can increase the external surface area and dramatically alter the diffusional properties of the zeolite materials [35–37]. Spectroscopic studies have revealed that silanol groups and EFAL species on the external surface are present in greater concentration in nanocrystalline NaY zeolite than in commercial NaY zeolite, because of the differences in external surface area [30,32]. (The external surface areas of nanocrystalline NaY and commercial NaY zeolite are 178 and ∼4 m^2/g, respectively [30].) Silanol groups and EFAL species on the external surface are responsible for the improved performance of nanocrystalline NaY zeolite in propylene-SCR of NO_2 [32]. In the present study, urea-SCR of NO_2 using nanocrystalline NaY zeolite as the catalyst led to a significantly greater SCR reaction rate and less formation of undesired products than seen in urea-SCR in commercial NaY.

The SCR reactions in nanocrystalline NaY zeolite occurred more quickly than in commercial NaY zeolite (Table 2). Consequently, higher NO_x conversion (Table 3) and NO_x^- conversion (Fig. 8a) was achieved in nanocrystalline NaY than in commercial NaY zeolite after urea-SCR for 2 h. The better SCR reaction rate in urea-SCR over nanocrystalline NaY zeolite can be explained by the greater concentrations of both silanol groups and EFAL sites than exist in commercial NaY. First, the silanol groups and EFAL species have diffusional advantages, because they both are located on the external surface of the nanocrystalline NaY zeolite. Furthermore, they are considered chemically distinct surface sites. A major conclusion of this study and previous studies is that nitrate adsorbed on EFAL sites on the external surface of nanocrystalline NaY zeolite is more reactive than nitrate in the internal pores adsorbed to Na^+ [32]. The activation of NH_3 by silanol groups is also important for N–N bond formation [2].

As shown in Scheme 1, EFAL species on nanocrystalline NaY zeolite also provide important sites for the adsorption and fast hydrolysis of HNCO, which is essential for avoiding isocyanic acid emission [15] and inhibiting the formation of undesired products, including biuret and cyanuric acid. The kinetic data listed in Table 2 indicate that the hydrolysis of HNCO occurred at much more rapidly in nanocrystalline NaY zeolite than in commercial NaY zeolite. This finding is consistent with the observation that gas-phase HNCO persists for a much longer period (>60 min; Fig. 5) in the presence of commercial NaY zeolite than in the presence of nanocrystalline NaY zeolite (<20 min; Fig. 4). The time course measurements for H_2O also indicate that hydrolysis occurs much faster in nanocrystalline NaY zeolite than in commercial NaY zeolite (Fig. 6c).

In conclusion, silanol groups and EFAL species are physically and chemically distinct surface sites present on the external surface of nanocrystalline NaY zeolite. These sites are responsible for the improved performance of nanocrystalline NaY relative to commercial NaY, because most urea-SCR reactions occur on the external surface. The role of the internal surface is to store NO_x before SCR reactions on the external surface. A pictorial representation of this multifunctional capability of the nanocrystalline zeolite catalyst is given in Scheme 2. Thus nanocrystalline alkali zeolites can be classified as new materials for SCR catalysts with potentially significantly better performance.

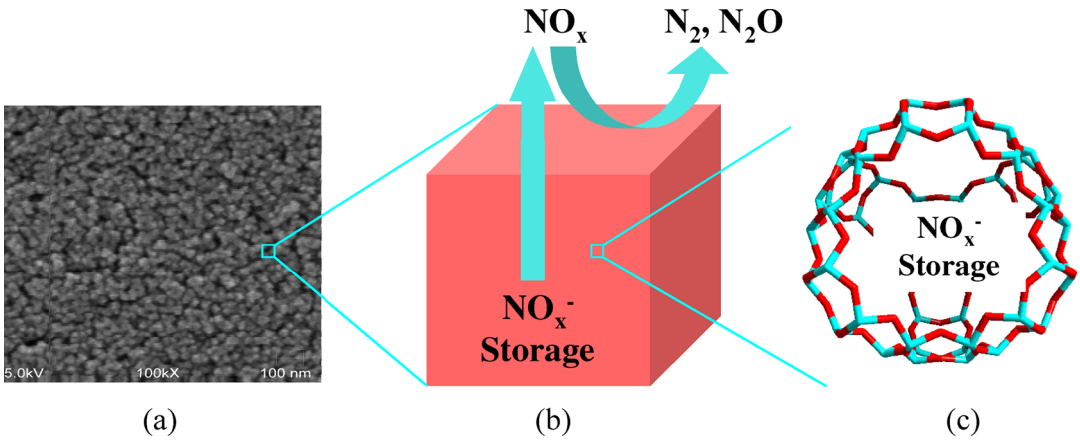

Scheme 2. (a) SEM image of nanocrystalline NaY zeolite (scale bar = 100 nm), (b) a nanocrystalline zeolite particle with a crystal size of 23 nm, and (c) zeolite Y supercage. The internal surface of nanocrystalline zeolite provides sites for NO_x storage (as nitarte and nitrite) and the minority of the SCR reactions, the external surface provides sites for additional NO_x storage and the majority of the SCR reactions.

4.4. Urea-SCR versus propylene-SCR of NO_2 in nanocrystalline NaY zeolite

An earlier study evaluated nanocrystalline NaY zeolite in deNO_x reactions at $T = 473$ K using propylene as the reducing agent and found that nanocrystalline NaY zeolite was very sensitive to preadsorbed water in propylene-SCR of NO_2 [32]. Compared with urea-SCR, propylene-SCR appears to be a less realistic deNO_x technology under typical conditions of humid, oxygen-rich exhaust streams [8,52].

Although we did not study the effect of adsorbed water on urea-SCR in the present work, water should not be detrimental to deNO_x with urea over nanocrystalline NaY zeolite. Water is necessary for the hydrolysis of HNCO in urea-SCR reactions (reaction (2)); moreover, as the above discussion suggests, at elevated temperatures water does not inhibit the adsorption of NH_3 in nanocrystalline NaY zeolite. In urea-SCR of NO_2 over nanocrystalline NaY zeolite, the concentration of H_2O in the gas phase kept increasing after the urea-SCR reactions were completed around $t = 40$ min (Fig. 6c). Fig. 6a indicates that the NH_3 concentration in the gas phase further decreased after $t = 40$ min. Because the oxidation of NH_3 by O_2 was not significant under the experimental conditions described in this work [17], NH_3 most likely adsorbed on available silanol groups and/or EFAL sites in nanocrystalline NaY zeolite in the presence of water [30,32].

Compared with urea-SCR, a significant amount of nitrate and carbonaceous deposit remained in nanocrystalline NaY zeolite after propylene-SCR of NO_2 at $T = 473$ K for 6 h [32]. The carbonaceous deposit in nanocrystalline NaY zeolite was found to hinder the adsorption of propylene and NO_2 and to further SCR reactions. In urea-SCR of NO_2 over nanocrystalline NaY zeolite, surface nitrate was not observed after 2 h of SCR reactions. Surface HNCO and OCN^- were the only undesired products formed in urea-SCR over nanocrystalline NaY (Fig. 8). Furthermore, more than 80% of NO_2 was converted into N_2 in urea-SCR relative to ∼20% selectivity to N_2 formation in propylene-SCR of NO_2 over nanocrystalline NaY zeolite [32]. As mentioned earlier, NO_x emissions emerge at high velocity under typical lean burn conditions [52]. At low temperature, urea-SCR over nanocrystalline NaY zeolite appears to be an even more promising deNO_x technology than propylene SCR.

5. Conclusions

Nanocrystalline NaY zeolite exhibits enhanced deNO_x at low temperature ($T = 473$ K) compared with commercial NaY zeolite, as demonstrated by the present study on the selective catalytic reduction of NO_2 with urea. Silanol groups and EFAL species on the external surface of nanocrystalline NaY were found to be responsible for the higher SCR reaction rate and decreased formation of undesired products, including biuret and cyanuric acid, relative to commercial NaY zeolite. Isotopic labeling coupled with FTIR analysis indicated that N–N bond formation involves both an N atom originating from NO_2 and an N atom originating from urea. In nanocrystalline NaY zeolite, kinetic studies suggests that NH_3 formed in thermal decomposition of urea was activated for SCR reactions by hydrogen bonding with silanol groups.

Nanocrystalline alkali zeolites can be considered as new catalytic materials that have NO_x storage capacity in the internal pores and high reactivity on the external surface. These features provide multifunctional capabilities beyond those found for zeolites with larger crystal size and smaller external surface area. Although for shape selective catalysis, the reactivity of the external surface may be undesirable, in reactions such as deNO_x or hydrocarbon cracking, nanocrystalline zeolite catalysts may have greatly enhanced reactivity because of reactions on the external surface. This is the first example in the literature demonstrating that the increased external surface area (up to ∼40% of the total surface area) of nanocrystalline zeolites can be used as a reactive surface with unique active sites for catalysis.

Acknowledgments

The authors thank Dr. Weiguo Song for providing the nanocrystalline NaY zeolite sample and the SEM image. Although the research described in this article was funded wholly or in part by the Environmental Protection Agency (grant EPA R829600 to S.C.L. and V.H.G.), it has not been subjected to the EPA's required peer and policy review. Thus this work does not necessarily reflect the views of the EPA, and no official endorsement should be inferred.

References

[1] S. Bhattacharyya, R.K. Das, Int. J. Energy Res. 23 (1999) 351.
[2] P. Forzatti, Appl. Catal. A 222 (2001) 221.
[3] B.K. Gullett, P.W. Groff, M. Lin, J.M. Chen, Air Waste 44 (1994) 1188.
[4] M. Koebel, M. Elsener, M. Kleemann, Catal. Today 59 (2000) 335.
[5] E. Seker, N. Yasyerli, E. Gulari, C. Lambert, R.H. Hammerle, Appl. Catal. B 37 (2002) 27.
[6] M. Koebel, E. Olav Strutz, Ind. Eng. Chem. Res. 42 (2003) 2093.
[7] R. van Helden, R. Verbeek, F. Willems, R. van der Welle, Soc. Automot. Eng. SP-1861 (2004) 25.
[8] P.L.T. Gabrielsson, Top. Catal. 28 (2004) 177.
[9] T. Morimune, H. Yamaguchi, Y. Yasukawa, Exp. Therm. Fluid Sci. 18 (1998) 220.
[10] D.H.E. Seher, M. Reichelt, S. Wickert, Soc. Automot. Eng. SP-1811 (2003) 21.
[11] P. Tennison, C. Lambert, M. Levin, Soc. Automot. Eng. SP-1860 (2004) 349.
[12] H.L. Fang, H.F.M. DaCosta, Appl. Catal. B 46 (2003) 17.
[13] S. Yim, S. Kim, J. Baik, I. Nam, Y. Mok, J. Lee, B. Cho, S. Oh, Ind. Eng. Chem. Res. 43 (2004) 4856.
[14] M. Larrubia, G. Ramis, G. Busca, Appl. Catal. B 27 (2000) L145.
[15] G. Delahay, B. Coq, Catal. Sci. Ser. 3 (2002) 345.
[16] C.A. Jones, D. Stec, S.C. Larsen, J. Mol. Catal. A 212 (2004) 329.
[17] J. Baik, S. Yim, I. Nam, Y. Mok, J. Lee, B. Cho, S. Oh, Top. Catal. 30 (2004) 37.
[18] R.Q. Long, R.T. Yang, J. Am. Chem. Soc. 121 (1999) 5595.
[19] R.Q. Long, R.T. Yang, J. Catal. 188 (1999) 332.
[20] R.Q. Long, R.T. Yang, J. Catal. 194 (2000) 80.
[21] F. Blatter, H. Sun, H. Frei, Catal. Lett. 35 (1995) 1.
[22] F. Blatter, H. Sun, S. Vasenkov, H. Frei, Catal. Today 41 (1998) 297.
[23] G. Li, M. Xu, S.C. Larsen, V.H. Grassian, J. Mol. Catal. A 194 (2003) 169.
[24] C. Sedlmair, B. Gil, K. Seshan, A. Jentys, J.A. Lercher, Phys. Chem. Chem. Phys. 5 (2003) 1897.
[25] Y. Yeom, J. Henao, M. Li, W.M.H. Sachtler, E. Weitz, J. Catal. 231 (2005) 181.
[26] M. Li, J. Henao, Y. Yeom, E. Weitz, W.M.H. Sachtler, Catal. Lett. 98 (2004) 5–9.
[27] Y.H. Yeom, B. Wen, W.M.H. Sachtler, E. Weitz, J. Phys. Chem. B 108 (2004) 5386.
[28] S.J. Schmieg, B.K. Cho, S. Oh, Appl. Catal. B 49 (2004) 113.
[29] M. Richter, A. Trunschke, U. Bentrup, K.W. Brzezinka, E. Schreier, M. Schneider, M.M. Pohl, R. Fricke, J. Catal. 206 (2002) 98.
[30] W. Song, G. Li, V.H. Grassian, S.C. Larsen, Environ. Sci. Technol. 39 (2005) 1214.
[31] G. Li, S.C. Larsen, V.H. Grassian, J. Mol. Catal. A 227 (2005) 25.
[32] G. Li, S.C. Larsen, V.H. Grassian, Catal. Lett., in press.
[33] E. Lukas, S. Decker, A. Khaleel, A. Seitz, S. Fultz, A. Ponce, W. Li, C. Carnes, K. Klabunde, Chem. Eur. J. 7 (2001) 2505.
[34] M. Ogura, T. Ohsaki, E. Kikuchi, Micropor. Mesopor. Mater. 21 (1998) 533.
[35] A. Shichi, K. Katagi, A. Satsuma, T. Hattori, Appl. Catal. B 24 (2000) 97.
[36] A. Shichi, A. Satsuma, T. Hattori, Appl. Catal. B 30 (2001) 25.
[37] T. Tabata, H. Ohtsuka, Catal. Lett. 48 (1997) 203.
[38] P. Praserthdam, N. Mongkolsiri, P. Kanchanawanichkun, Catal. Commun. 3 (2002) 191.
[39] Q. Li, D. Creaser, J. Sterte, Chem. Mater. 14 (2002) 1319.
[40] J. Szanyi, J. Kwak, R.A. Moline, C.H.F. Peden, Phys. Chem. Chem. Phys. 5 (2003) 4045.
[41] J. Szanyi, J. Kwak, C.H.F. Peden, J. Phys. Chem. B 108 (2004) 3746.
[42] U. Eickhoff, F. Temps, Phys. Chem. Chem. Phys. 1 (1999) 243.
[43] A. Lapinski, J. Spanget-Larsen, J. Waluk, J. Radziszewski, J. Chem. Phys. 115 (2001) 1757.
[44] R.E. Baren, M.A. Erickson, J.F. Hershberger, Int. J. Chem. Kinet. 34 (2002) 12.
[45] P.W. Beck, K. Feldl, Angew. Chem. Int. Ed. 5 (1966) 722.
[46] M.S. Lowenthal, R.K. Khanna, M.H. Moore, Spectrochim. Acta Part A 58 (2002) 73.
[47] N.B. Colthup, L.H. Daly, S.E. Wiberley, Introduction to Infrared and Raman Spectroscopy, Chapmann & Hall, London, 1990.
[48] N.W. Cant, D.C. Chambers, A.D. Cowan, I.O.Y. Liu, A. Satsuma, Top. Catal. 10 (2000) 13.
[49] D.T. Burns, A. Townshend, A.H. Carter, Reactions of the Elements and Their Compounds (Part A), Inorganic Reaction Chemistry, vol. 2, Horwood, Chichester, 1981.
[50] P.A.S. Smith, The Organic Chemistry of Open-Chain Nitrogen Compounds, vol. I, 1965.
[51] T.G. Koch, N.S. Holmes, T.B. Roddis, J.R. Sodeau, J. Chem. Soc., Faraday Trans. 92 (1996) 4787.
[52] J.N. Armor, Catal. Today 26 (1995) 99.